Editors' Suggestion

# Using Andreev bound states and spin to remove domain walls in a Kitaev chain

Wietze D. Huisman,* Sebastiaan L. D. ten Haaf,* Chun-Xiao Liu, Qingzhen Wang, Alberto Bordin, Florian J. Bennebroek Evertsz', Bart Roovers, Michael Wimmer, and Srijit Goswami†
*QuTech and Kavli Institute of Nanoscience, Delft University of Technology, 2600 GA Delft, The Netherlands*

(Received 21 January 2026; revised 26 June 2026; accepted 21 September 2026; published 3 November 2026)

Quantum dot (QD)-superconductor hybrids have been established as a suitable platform for realizing Kitaev chains hosting Majorana bound states. Implementing these structures in a qubit architecture is expected to result in coherence times that scale exponentially with the lengths of the chains. To scale to longer systems, the phase differences between all superconducting segments in the chain need to be controlled. While this control has been demonstrated by using an external magnetic flux [ten Haaf *et al.*, Nature (London) **641**, 890 (2025); Bordin *et al.*, Nat Commun **17**, 2313 (2026)], ideally, it can be achieved with control over intrinsic system parameters [Liu *et al.*, Phys. Rev. Res. **7**, L012045 (2025)]. In this work, we investigate whether the relevant phase differences can be tuned through the spin degree of freedom in each QD or the chemical potential of the discrete bound states in the hybrid sections. We confirm that both these tuning knobs allow for controlling the phase difference in the couplings between neighboring QDs, bypassing the requirement to tune an external flux. However, we find that the amplitude of the phase shifts can deviate from a discrete $\pi$ shift. We introduce a spatial variation in the spin-orbit field as a possible mechanism to explain the observed behavior and comment on the consequences for experimentally creating long Kitaev chains.

DOI: 10.1103/2fyb-mpp9

## I. INTRODUCTION

The Kitaev chain models a one-dimensional (1D) spinless fermionic chain with a *p*-wave superconducting pairing, which hosts unpaired Majoranas at its edges [1]. These quasiparticles are central to many schemes for fault-tolerant quantum computation [2,3]. Semiconductor quantum dots (QDs) coupled via superconductors offer an experimentally tunable realization of the Kitaev chain [4–7], which has so-far enabled the creation of localized Majoranas in systems with two-QD [8–10] and three-QD [11,12] sites. The protection of Majoranas against perturbations scales with the number of sites in the chain, making it highly desirable to extend these arrays. Scaling to longer chains would, for instance, enable implementations of a parity qubit with longer coherence times [5,12,13] or demonstrations of the non-Abelian exchange of Majorana quasiparticles [13–16]. A fundamental obstacle for scaling to longer chains is posed by phase differences that arise between neighboring superconductors. In a Kitaev chain, any $\pi$-phase difference between neighboring superconducting pairings locally closes the excitation gap. This effectively cuts the chain in segments as a so-called domain wall is formed [1,4]. One ideally requires all phases to be uniform. Authors of recent works on three-site systems have addressed this problem via a flux-controlled superconducting loop [11,17]. This is, however, not a practical solution for longer systems: an *N*-site chain would require independent control over the flux through *N*-2 superconducting loops.

It was recently proposed [18] that Kitaev chains could in fact be scaled without explicit flux control. Instead, control over the spin configuration of the QDs and/or control over the chemical-potential energy of the hybrid segments was predicted to be sufficient to achieve this. Here, we investigate this strategy experimentally by studying a three-site Kitaev chain in an InSbAs two-dimensional electron gas (2DEG) with a flux-tunable superconducting loop. We follow the protocol in Ref. [11] to create localized Majorana edge modes and study the flux response of the excitation gap in the middle QD. By comparing the response to the superconducting flux for different spin configurations, we confirm that changing the spin polarization of one of the QDs introduces a discrete phase shift in the system. Furthermore, we show that changing the chemical potential energy of one of the hybrid segments induces a similar phase shift, providing a second mechanism that can remove a domain wall. Closer inspection reveals that the phase shifts evolve smoothly as a function of the Andreev bound state (ABS) charge, which can result in sweet spots with an arbitrary (non-$\pi$) difference in their relative phase. We theoretically analyze how an effective spatial variation in the spin-orbit field gives rise to the smooth phase evolution and derive an analytical expression to compare with the experimental results. Our results show that flux-free scaling of the Kitaev chain can be feasible but that a deeper understanding of microscopic details of the system is important for implementing the technique.

*These authors contributed equally to this work.
†Contact author: s.goswami@tudelft.nl

*Published by the American Physical Society under the terms of the Creative Commons Attribution 4.0 International license. Further distribution of this work must maintain attribution to the author(s) and the published article's title, journal citation, and DOI.*

### A. The scaling protocol

The Hamiltonian for the general $N$-site Kitaev chain is given by [1,4]

$$H = \sum_{j}^{N} \mu_j c_j^\dagger c_j + \sum_{j}^{N-1} \left( t_j c_j^\dagger c_{j+1} + |\Delta_j| e^{-i\phi_j} c_j^\dagger c_{j+1}^\dagger \right) + \text{H.c.}$$

A gauge transformation allowed for taking the chemical potentials $\mu_j$ and hopping terms $t_j$ to be real and assigning a complex phase $\phi_j$ only to the superconducting pairings $\Delta_j$ [1,19]. In a 1D system with Rashba spin-orbit coupling, these phases are restricted so that $\phi_j$ is either 0 or $\pi$ [4]. For any $N$, unpaired Majoranas arise on the two outermost sites when $\mu_j = 0$, $|t_j| = |\Delta_j|$; this is referred to as the Majorana sweet spot. When all phases are equal (such that either all $t_j = +\Delta_j$ or all $t_j = -\Delta_j$), the middle sites host an excitation gap that separates the Majorana modes at the edge. The Kitaev chain can be effectively engineered by coupling spin-polarized QDs via ABSs in a semiconductor-superconductor hybrid segment [8,9,13]. Focusing first on a minimal two-site system, the hopping interaction ($t$) occurs through elastic cotunneling (ECT), whereas crossed Andreev reflection (CAR) provides a pairing interaction ($\Delta$) via the creation or splitting of Cooper pairs in the superconductor [20,21] [Fig. 1(a)]. Crucially, the amplitudes $t$, $\Delta$ of these virtual processes depend differently on the ABS chemical potential energy $\mu_{\text{ABS}}$. Additionally, the relative signs of the amplitudes are affected by the spin configuration of the spin-polarized QDs. Depending on whether the spins of the QDs are aligned or antialigned, either the CAR or the ECT process requires the presence of spin-orbit interactions. As a result, the coupling mechanism differs for different spin configurations. Figure 1(b) shows theoretically calculated $t$, $\Delta$ amplitudes as a function of $\mu_{\text{ABS}}$, previously shown in Ref. [18], comparing an equal spin alignment and an opposite spin alignment in the QDs. For each spin configuration, tuning $\mu_{\text{ABS}}$ enables either $t = +\Delta$ or $t = -\Delta$. Focusing on $\mu_{\text{ABS}} < 0$, changing the spin of one of the QDs similarly changes the relative amplitude from $t = +\Delta$ to $t = -\Delta$ (vice versa for $\mu_{\text{ABS}} > 0$). The relative sign between $t$, $\Delta$ becomes relevant when considering a Kitaev chain with $N \geqslant 3$ QD sites. To see this, we turn to a spinful model considering three spinful QDs and two ABSs (see Supplemental Material [22]). Figure 1(c) shows numerical conductance spectra of the middle QD at a three-site sweet spot, as a function of the phase difference $\phi$ between the two superconducting pairings. For the left spin configuration, for example, we find a situation where the gap is closed when $\phi = 0$ due to the formation of a domain wall. Changing the spin on the right QD shifts the entire spectrum by a $\pi$ phase, removing the domain wall and reopening the excitation gap in the middle QD at $\phi = 0$.

### B. Device and measurement setup

A schematic overview and a scanning electron micrograph (SEM) of the measured device are shown in Figs. 1(d) and 1(e). Three large lithographically defined depletion gates (red) confine a narrow conductance channel across two superconducting strips (green). Narrow gates are used to define three QDs on the left, in the middle, and on the right of the two superconducting regions. Their chemical potential energies

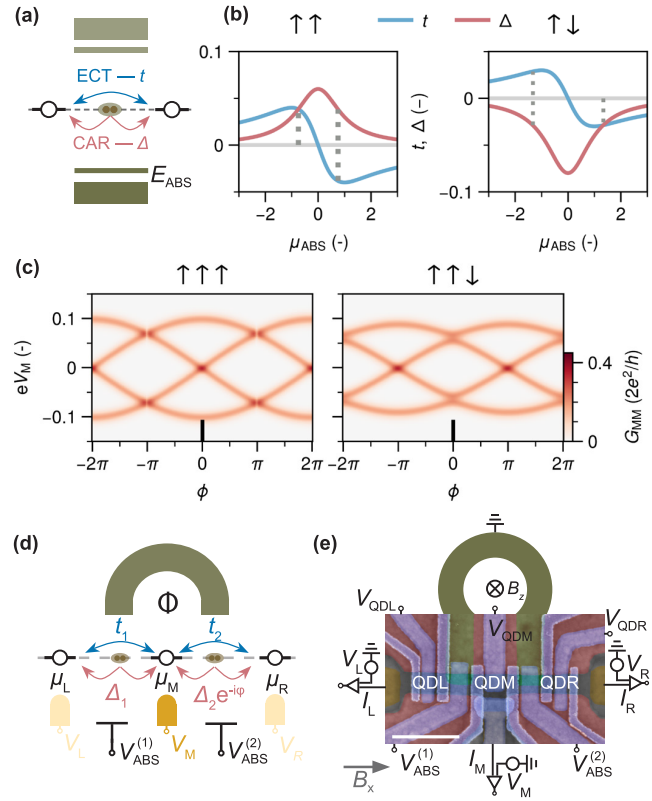



FIG. 1. Proposed mechanisms for controlling phase in the Kitaev chain and device layout of a three-site chain. (a) Schematic of ECT and CAR subgap processes in a two-site Kitaev chain setup, controlled by an ABS with energy $E_{\text{ABS}}$. (b) ECT ($t$) and CAR ($\Delta$) amplitudes as a function of $\mu_{\text{ABS}}$ for two different spin configurations. (c) Simulated conductance spectra on the middle QD of a three-site Kitaev chain as a function of the phase $\phi$. Two different spin configurations are compared, demonstrating the removal of a domain wall through flipping the rightmost spin. (d) Three-site Kitaev chain schematic showing the two pairs of couplings $t_1$, $\Delta_1$ and $t_2$, $\Delta_2$. Phase modulation is enabled by threading a flux $\Phi$ through the superconducting loop connecting the two hybrid sections. (e) Scanning electron micrograph (SEM) of the measured device. An out-of plane magnetic field $B_z$ is used to modulate the flux, with a period of 28 μT. An in-plane magnetic field $B_x$ is applied parallel to the channel to spin-polarize the QDs.

are controlled by $V_{\text{QDL}}$, $V_{\text{QDM}}$, and $V_{\text{QDR}}$, respectively. The two hybrid sections host discrete ABSs [11], whose energies are controlled by $V^{(1)}_{\text{ABS}}$ and $V^{(2)}_{\text{ABS}}$. The sections are connected in a loop, enabling an out-of-plane magnetic field $B_z$ to control the flux $\Phi$ through the loop. This directly controls the relative phases of the interdot couplings between neighboring QD pairs [11,17]. Each QD is coupled to a normal contact via a tunneling barrier, allowing us to probe the local density of states at the edges and in the middle of the chain. Fast measurements are performed using radiofrequency lead reflectometry techniques enabled by off-chip lumped-element resonators, where the reflected phase and amplitude of signal $S^i_{21}$ on lead $i$ is recorded. We plot the processed signal $\widetilde{S}^i_{21}$, as detailed in the Supplemental Material [22]. In addition, we

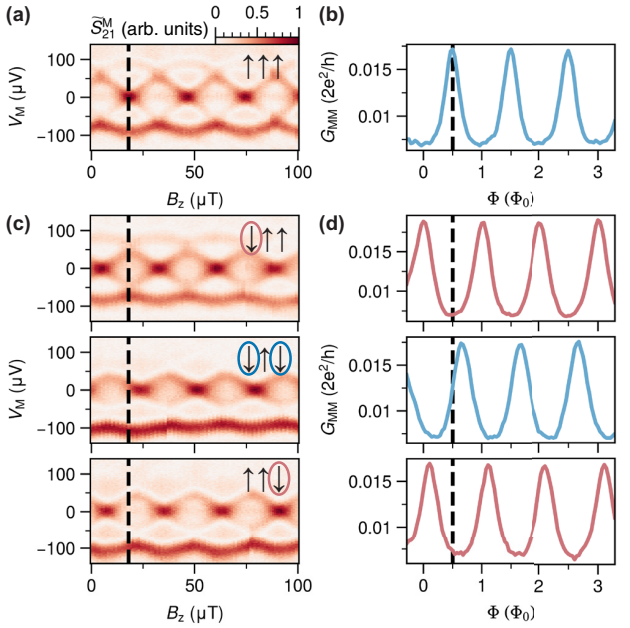



FIG. 2. Spin-induced phase shifts. (a) Bias spectroscopy measurement for the middle QD as a function of the out-of-plane magnetic field $B_z$ for an ↑↑↑ spin configuration. (b) A higher-resolution $G_{MM}$ linetrace along $V_M = 0$, expressed in units of the flux quantum $\Phi_0$. We identify a flux where the excitation gap closes. (c) Repeated measurements of (a), for different spin configurations. (d) Comparison of $G_{MM}$ linetraces along $V_M = 0$, for the same spin configurations as in (c). Applied magnetic field along $B_x$ is 150 mT. The behavior is reproducibly observed, shown in Fig. S2 in the Supplemental Material [22].

show measurements of the differential conductance $G_{MM} = \frac{dI_M}{dV_M}$ through the middle ohmic contact.

## II. RESULTS

### A. Spin-induced phase shift

To initialize the system, we identify an isolated orbital in each of the three QDs. An in-plane magnetic field ($B_x$) is applied along the length of the 1D channel to spin-polarize the QDs (Fig. S1 in the Supplemental Material [22]). Since each orbital has two spin polarizations, we can study eight different combinations of resonances. We use the combined spin configuration as label. Following the same protocol as in our previous work [11], the device is first tuned up so that the condition $|t_i| = |\Delta_i|$ is satisfied for each of the two QD pairs (left/middle and middle/right). This is achieved by tuning $V^{(1)}_{ABS}$ and $V^{(2)}_{ABS}$ to change the charge and energy of ABSs, which in turn affects the interdot couplings [see Figs. 1(b) and 1(c)]. The tune-up is completed by setting all $V_{QDi}$ values to the charge degeneracy point corresponding to $\mu_i = 0$. To identify the flux corresponding to a phase $\phi = 0$, we measure the finite-bias conductance through the middle QD $G_{MM}$ as a function of $B_z$ [Fig. 2(a)]. The excitation gap in the middle QD closes periodically as a function of $B_z$, in line with the predicted behavior shown in Fig. 1(c) and Refs. [11,17,18]. The value of $B_z$ where the excitation gap in the middle QD closes is taken as a reference point (indicating $\phi = \pi$), which can be easily extracted from a measurement along $V_M = 0$ [Fig. 2(b)].

The result in Fig. 2(a) is obtained for an ↑↑↑ spin configuration. We can select a different spin configuration through the voltages $V_{QDi}$. For each adjustment, a slight retuning of $V_{ABS}$ is required to maintain the $|t_i| = |\Delta_i|$ condition. We repeat the measurement in Fig. 2(a) for three different combinations of spin polarizations of the outer QDs, shown in Fig. 2(c). For every adjustment of a spin polarization, we observe that the spectrum shifts by approximately half a flux period, corresponding to a $\pi$ shift in the effective phase $\phi$. To compare the flux response more closely, we compare linetraces along $V_M = 0$ in Fig. 2(d). Focusing on the $\Phi$ value indicated by the dashed line, at fixed $B_x$, the excitation gap in the system is either present or closed depending on the spin configuration. This, in principle, demonstrates the desired control: The spin configuration serves as a tool to remove a domain wall, without requiring to tune the external flux. We note, however, that small offsets from $\phi = 0$ or $\phi = \pi$ appear in the bottom two configurations, marking a departure from the discrete $0/\pi$ shift presented in Fig. 1(c). This motivates a more in-depth study where we turn to the second predicted control knob: the ABS charge.

### B. ABS-induced phase shift

The charge of the ABSs provides a second way to change the relative sign of the $t$ and $\Delta$ amplitudes, as highlighted in Fig. 1(b). Hence, tuning between the two available $|t| = |\Delta|$ sweet spots within the range of a single ABS should yield a relative phase shift while maintaining the same spin configuration. In contrast with changing the spin of the QDs, this control via $V_{ABS}$ allows for a continuous interpolation between two sweet spots. First, we search for a range in $V^{(2)}_{ABS}$ where the rightmost QD interacts with a single ABS. Figure 3(a) shows a charge stability diagram of two spin-polarized resonances in the right QD interacting with an ABS in the right hybrid segment. As $V^{(2)}_{ABS}$ is varied, the positions of the QD resonances are modulated, indicating interaction with ABSs in this range [23]. Here, we find that one sweet spot can be clearly identified for the spin-down resonance, while the spin-up resonance allows for determining a sweet spot at two different ABS energies (Fig. S4 in the Supplemental Material [22]). At each of these three sweet spots, we obtain a zero-bias conductance measurement as a function of flux, shown in Fig. 3(b). Comparing these linetraces, we observe that now the changes in both the spin and the ABS energy result in comparable relative phase shifts. Next, we study the flux dependence of the system throughout a larger range of $V^{(2)}_{ABS}$ around the two spin-up sweet spots to interpolate how the system evolves from the result in Fig. 3(b)(ii) to the shifted trace in Fig. 3(b)(iii). Generally then, $|t_2| \neq |\Delta_2|$, while we maintain $|t_1| = |\Delta_1|$. Similar to Fig. 3(b), we characterize the flux dependence by measuring the response of the zero-bias conductance. The oscillations are fitted to estimate the value $B_z$ where the excitation gap closes (see Fig. S3 in the Supplemental Material [22]), which allows us to extract a single value $\widetilde{\Phi}$ that characterizes the relative flux shift at each $V^{(2)}_{ABS}$ point with respect to the dashed line in Fig. 3(b)(i). The evolution of this extracted flux shift $\widetilde{\Phi}$ vs the ABS energy is

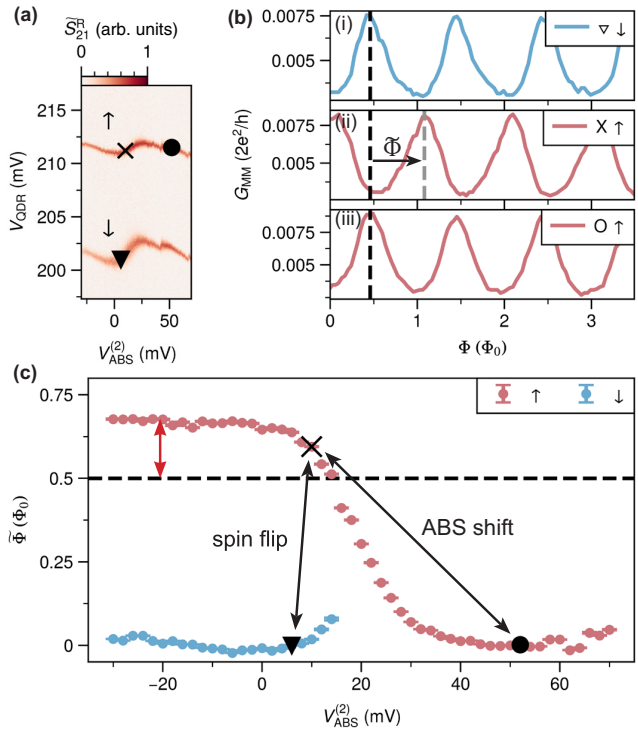



FIG. 3. ABS-induced phase shifts. (a) Hybridization between the right ABS and two spin levels of the right QD QDR. Three sweet spots ($\times, \circ, \triangledown$) are identified from charge stability diagrams of the right and middle QD (Fig. S4 in the Supplemental Material [22]). (b) Flux dependence of the zero-bias conductance $G_{\mathrm{MM}}$ on the middle dot, measured at the three sweet spots indicated in (a). (c) Continuous measurement of the extracted flux shift $\widetilde{\Phi}$ as a function of the right ABS energy. The extracted shift $\widetilde{\Phi}$ is defined with respect to the first conductance peak in the zero-bias trace as indicated in (b) (see Fig. S3 in the Supplemental Material [22] for further details about the extraction). The spin-down configuration is only shown for values of $V_{\mathrm{ABS}}^{(2)} < 16\,\mathrm{mV}$, as the extraction was unreliable for the rest of the range. Raw datasets are shown in Figs. S6 and S7 in the Supplemental Material [22]. Measurements were performed at an in-plane field $B_x$ of 200 mT. The flux dependence of the energy spectrum at all values of the ABS energy is shown in Fig. S5 in the Supplemental Material [22].

shown in Fig. 3(c). The extracted flux shift in Fig. 3(c) reveals three important observations. First, we find that the flux shift induced by a spin flip is similar to the flux shift acquired by changing the ABS charge from one sweet spot to another. This indicates that the underlying mechanism shown in Fig. 1(b) appears to be well understood. However, we also observe that the flux shift, and therefore the phase, varies smoothly between two sweet spots as the ABS energy is changed, deviating from the scenario where only phases of 0 or $\pi$ appear in the system [4]. Given that the exact positions of the two sweet spots along $V_{\mathrm{ABS}}$ depend on underlying microscopic details, a smooth phase evolution means that any arbitrary flux shift can appear in practice. Furthermore, the phase separation of the plateaus at the extremes of the ABS range is larger than $\pi$, indicated by the red arrow. The practical implications of this are treated in the Discussion. Below, we address how the model underlying Fig. 1(c) can be adjusted to reproduce this behavior.

### C. Possible origin of the smooth phase evolution

The above results deviate from the original theoretical result [18] in two clear ways: The system smoothly interpolates between two phase plateaus as a function of $V_{\mathrm{ABS}}^{(2)}$, and the separation of the two plateaus corresponds to a total phase shift larger than $\pi$. In a system that respects complex conjugation symmetry, only discrete 0 or $\pi$ phases arise. A possible mechanism that could break this symmetry is a spatial variation in the effective spin-orbit field along the chain, which was so far assumed to be fixed perpendicular to the chain. As a starting point, we present here a simple adjustment to the model underlying Fig. 1(c) that implements this by introducing an in-plane offset angle $\theta_{\mathrm{A}}$ between the polarization axis of the QDs ($\vec{B}_{\mathrm{QD}}$) and that of the ABS ($\vec{B}_{\mathrm{ABS}}$), with Zeeman energy $E_{\mathrm{Z}}^{\mathrm{ABS}}$. This is equivalent to a specific configuration of a spatially varying spin-orbit field $\vec{B}_{\mathrm{SO}}$, treated more generally in the Supplemental Material [22]. Mapping the full model onto an effective three-site model allows us to obtain an expression for the complex phase-shift $\widetilde{\phi}$ in the system (see Supplemental Material [22]) as a function of ABS parameters

$$\widetilde{\phi} = \frac{\pi}{2} - \arctan\left[\frac{\mu_{\mathrm{ABS}} + \mu_0\left(\theta_{\mathrm{A}}, E_{\mathrm{Z}}^{\mathrm{ABS}}\right)}{\Gamma\left(\theta_{\mathrm{A}}, E_{\mathrm{Z}}^{\mathrm{ABS}}\right)}\right]. \tag{1}$$

When $\theta_{\mathrm{A}}, E_{\mathrm{Z}}^{\mathrm{ABS}} = 0$, the dependence on $\mu_{\mathrm{ABS}}$ is a step function between 0 and $\pi$, centered around $\mu_{\mathrm{ABS}} = 0$. The parameter $\Gamma \propto E_{\mathrm{Z}}^{\mathrm{ABS}} \sin(\theta_{\mathrm{A}})$ smoothens the step function, and $\mu_0 \propto E_{\mathrm{Z}}^{\mathrm{ABS}} \cos(\theta_{\mathrm{A}})$ shifts the center of the curve away from $\mu_{\mathrm{ABS}} = 0$. In Fig. 4(a), we show the dependence on $\mu_{\mathrm{ABS}}$ for varying $\theta_{\mathrm{A}}$ at fixed $E_{\mathrm{Z}}^{\mathrm{ABS}}$, highlighting the smoothening effect on the step function when $\theta_{\mathrm{A}} \neq 0$. The scattered points indicate the two values of $\mu_{\mathrm{ABS}}$ that numerically correspond to sweet spots. Due to the smoothening, the phase separation between the two sweet spots decreases as a function of $\theta_{\mathrm{A}}$ and $E_{\mathrm{Z}}^{\mathrm{ABS}}$ [Fig. 4(b)], as they lie more toward the center of the smoothened curve, similar to Fig. 3(c). A plot of $\Gamma$ as a function of $\theta_{\mathrm{A}}$ is shown for two values of $E_{\mathrm{Z}}^{\mathrm{ABS}}$ in Fig. 4(c), where we see that the broadening is maximum when $\theta_{\mathrm{A}} = \pi/2$. Fitting the result Eq. (1) to the experimental data captures the overall trend well (Fig. S5 in the Supplemental Material [22]). We stress, however, that the larger-than-$\pi$ separation of the plateaus in Fig. 3(c) is not directly described by this mechanism.

## III. DISCUSSION

The key finding of this work is that both QD spin and ABS charge can affect the phase of a superconducting pairing in a Kitaev chain device and hence serve as a tuning knob to remove domain walls. We observe, however, that a continuous range of phases can arise, contrasting original predictions that the phase should be restricted to 0 or $\pi$. In our model, we find that spatial variations in the alignment of the spin-orbit field can be a possible explanation for these deviations, previously not explicitly included in models of this system. We believe this to be a physically reasonable assumption, which may

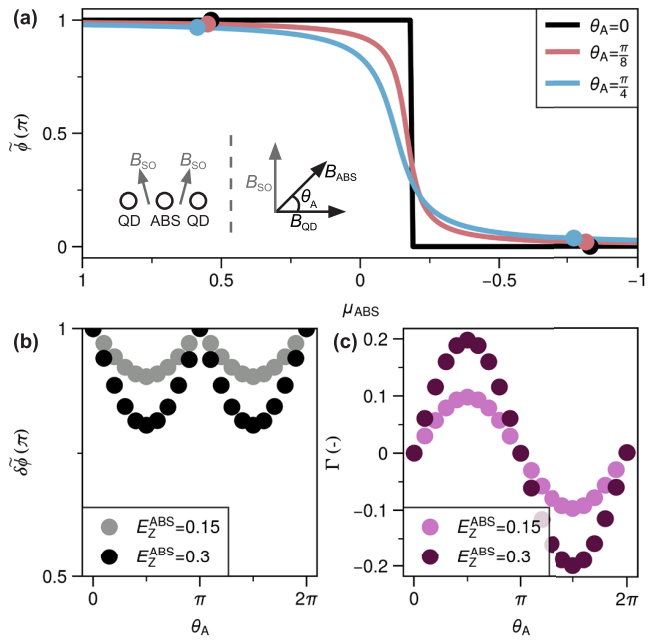



FIG. 4. Theoretical analysis of $\widetilde{\phi}$ as a function of $\mu_{\mathrm{ABS}}$. (a) To explain the experimental result, we propose a spatial variation in the spin-orbit hopping between neighboring sites as possible source (inset left). We implement this here equivalently through an offset angle $\theta_{\mathrm{A}}$ between the polarization of the QDs and the ABS (inset right). The more general case is discussed in the Supplemental Material [22]. The analytically obtained phase shift $\widetilde{\phi}$ [Eq. (1)] is plotted, for various $\theta_{\mathrm{A}}$. For each curve, the two $\mu_{\mathrm{ABS}}$ values are indicated that correspond to a sweet spot numerically. A fitting of the experimental data to the theoretical result is shown in Fig. S5 in the Supplemental Material [22]. (b) The smoothening of the phase dependence on $\mu_{\mathrm{ABS}}$ results in a decrease in the phase difference $\delta\widetilde{\phi}$ between two sweet spots for two values of $E_Z^{\mathrm{ABS}}$ in units of the induced superconducting pairing in the ABS. While $\theta_{\mathrm{A}}$ is not easily accessible in an experiment, we show a similar decrease in the phase difference as the global polarizing field is rotated in Fig. S9 in the Supplemental Material [22]. (c) The smoothening parameter $\Gamma$ as a function of $\theta_{\mathrm{A}}$ for two values of $E_Z^{\mathrm{ABS}}$.

arise through variations in the electrical fields or microscopic differences in the QDs/tunnel barriers. An anisotropic $g$ tensor along the chain could also produce this, although the in-plane $g$ factor is expected to be isotropic in our material [24]. We speculate that the observed larger-than-$\pi$ shifts may arise if the spin-orbit field itself is affected by the $V_{\mathrm{ABS}}$ gate voltage or through the presence of multiple ABSs. To minimize the deviations induced by spin-orbit misalignments, this effect should be considered in the design of future experiments. Specifically, our results suggest that complex geometries for applications such as braiding experiments should consist of predominantly parallel chains, allowing a single field $\vec{B}$ to be perpendicular to $\vec{B}_{\mathrm{SO}}$ everywhere.

The main purpose of the investigated protocol is the removal of domain walls in long Kitaev chains without requiring an external flux. In this regard, it should be stressed that our findings indicate the protocol is not optimal: While the $V_{\mathrm{ABS}}$ knob allows for continuous control over the superconducting phase, the devices are operated at specific sweet spots in this parameter space. Under realistic circumstances, we therefore believe both spin and ABS will be able to tune away from $\phi = \pi$ but not exactly to the ideal $\phi = 0$ configuration. The main consequence of this is that the excitation gap on the middle site will be reduced compared with its maximum value when the effective phase $\phi = 0$. As an example, we show this reduction explicitly in Fig. S8 in the Supplemental Material [22], where we quantitatively analyze the decrease in the excitation gap for the results shown in Fig. 2. By extracting the phases of the $\downarrow\uparrow\uparrow$ and $\downarrow\uparrow\downarrow$ configurations in Fig. 2, we find that the phase difference between the states deviates from $\pi$ by approximately 30% or 4 $\mu$T (Fig. S10 in the Supplemental Material [22]). This in turn leads to a decrease in the excitation gap from approximately 50 to 38 $\mu$eV. A larger deviation from $\pi$ translates directly to a larger reduction in the energy gap. However, if the phase shift is nonzero, it may be used to avoid a situation where the excitation gap closes. Compared with fine-tuned flux control over multiple loops, with the drawbacks of requiring additional control lines and accounting for cross-talk [25,26], we believe this presented technique to be the preferred alternative.

## IV. CONCLUSIONS

We have studied the phase-dependent energy spectra of different spin configurations of a three-site Kitaev chain. Through flux-dependent measurements, we observe that phase shifts close to $\pi$ can be achieved by changing the spin occupation on either of the outer QDs. These phase shifts would allow to avoid domain walls, enabling the scaling to longer Kitaev chains without the need for external flux control. Interestingly, upon further investigation, we find that the relative phase varies smoothly with the ABS charge, which can give rise to arbitrary phase shifts between sweet spots. We theoretically show that a spatial variation in the spin-orbit field can be a possible mechanism for the observed continuous transition. This finding helps to understand the origin of phase shifts that deviate from $\pi$ and conditions under which the spin-flip protocol can be used reliably in future experiments. The focus of this work has been to study how the combination of superconducting phase difference, electron spin, and spin-orbit coupling affects the scaling of Kitaev chains. We note that the interplay between these degrees of freedom determines the underlying physics of a wide variety of superconductor-semiconductor hybrid materials and devices that are actively being researched, such as superconducting germanium [27,28], multiterminal Josephson junctions [29,30], and Andreev spin qubits [31–33].

## ACKNOWLEDGMENTS

We thank C. Thomas, D. Xiao, and M. J. Manfra for the provision of the 2DEG materials. We thank O. W. B. Benningshof, T. Orton, and J. D. Mensingh for technical assistance with the cryogenic electronics. We thank S. Miles and J. L. Torres for their input on the theoretical analysis. We are grateful to I. Kulesh, C. G. Prosko, and Y. Zhang for developing the resonator circuits and high-frequency setup. The research at Delft was supported by the Dutch National Science Foundation (NWO), Microsoft Corporation Station Q, and a grant

from Top consortium for Knowledge and Innovation program (TKI). S.G. and M.W. acknowledge financial support from the Horizon Europe Framework Program of the European Commission through the European Innovation Council Pathfinder Grant No. 101115315 (QuKiT).

Q.W. fabricated the device. Measurements were performed by W.D.H. and S.L.D.t.H. Theoretical analysis was provided by C-X.L., S.L.D.t.H., and M.W. A.B., F.J.B.E., and B.R. helped interpret the experiments to understand the phase behavior. The manuscript was written by W.D.H. and S.L.D.t.H. with input from all coauthors. S.G. supervised the experimental work in Delft.

## DATA AVAILABILITY

All raw data obtained in relation to this manuscript and the scripts to produce the figures are available on Zenodo [34].


[1] A. Y. Kitaev, Unpaired Majorana fermions in quantum wires, Phys. Usp. **44**, 131 (2001).

[2] A. Kitaev, Fault-tolerant quantum computation by anyons, Ann. Phys. **303**, 2 (2003).

[3] C. Nayak, S. H. Simon, A. Stern, M. Freedman, and S. Das Sarma, Non-Abelian anyons and topological quantum computation, Rev. Mod. Phys. **80**, 1083 (2008).

[4] J. D. Sau and S. D. Sarma, Realizing a robust practical Majorana chain in a quantum-dot-superconductor linear array, Nat. Commun. **3**, 964 (2012).

[5] M. Leijnse and K. Flensberg, Parity qubits and poor man's Majorana bound states in double quantum dots, Phys. Rev. B **86**, 134528 (2012).

[6] I. C. Fulga, A. Haim, A. R. Akhmerov, and Y. Oreg, Adaptive tuning of Majorana fermions in a quantum dot chain, New J. Phys. **15**, 045020 (2013).

[7] A. Tsintzis, R. S. Souto, and M. Leijnse, Creating and detecting poor man's Majorana bound states in interacting quantum dots, Phys. Rev. B **106**, L201404 (2022).

[8] T. Dvir, G. Wang, N. van Loo, C. X. Liu, G. P. Mazur, A. Bordin, S. L. D. ten Haaf, J. Y. Wang, D. van Driel, F. Zatelli, *et al.*, Realization of a minimal Kitaev chain in coupled quantum dots, Nature (London) **614**, 445 (2023).

[9] S. L. D. ten Haaf, Q. Wang, A. M. Bozkurt, C.-X. Liu, I. Kulesh, P. Kim, D. Xiao, C. Thomas, M. J. Manfra, T. Dvir, *et al.*, A two-site Kitaev chain in a two-dimensional electron gas, Nature (London) **630**, 329 (2024).

[10] F. Zatelli, D. van Driel, D. Xu, G. Wang, C.-X. Liu, A. Bordin, B. Roovers, G. P. Mazur, N. van Loo, J. C. Wolff, *et al.*, Robust poor man's Majorana zero modes using Yu-Shiba-Rusinov states, Nat. Commun. **15**, 7933 (2024).

[11] S. L. D. ten Haaf, Y. Zhang, Q. Wang, A. Bordin, C.-X. Liu, I. Kulesh, V. P. M. Sietses, C. G. Prosko, D. Xiao, C. Thomas, *et al.*, Observation of edge and bulk states in a three-site Kitaev chain, Nature (London) **641**, 890 (2025).

[12] A. Bordin, C.-X. Liu, T. Dvir, F. Zatelli, S. L. D. ten Haaf, D. van Driel, G. Wang, N. van Loo, Y. Zhang, J. C. Wolff, *et al.*, Enhanced Majorana stability in a three-site Kitaev chain, Nat. Nanotechnol. **20**, 726 (2025).

[13] A. Tsintzis, R. S. Souto, K. Flensberg, J. Danon, and M. Leijnse, Majorana qubits and non-Abelian physics in quantum dot–based minimal Kitaev chains, PRX Quantum **5**, 010323 (2024).

[14] S. Krøjer, R. Seoane Souto, and K. Flensberg, Demonstrating Majorana non-Abelian properties using fast adiabatic charge transfer, Phys. Rev. B **105**, 045425 (2022).

[15] P. Boross and A. Pályi, Braiding-based quantum control of a Majorana qubit built from quantum dots, Phys. Rev. B **109**, 125410 (2024).

[16] S. Miles, F. Zatelli, A. M. Bozkurt, M. Wimmer, and C.-X. Liu, Braiding Majoranas in a linear quantum dot–superconductor array: Mitigating the errors from Coulomb repulsion and residual tunneling, Phys. Rev. B **113**, 085302 (2026).

[17] A. Bordin, F. J. B. Evertsz', B. Roovers, J. D. T. Luna, W. D. Huisman, F. Zatelli, G. P. Mazur, S. L. D. ten Haaf, G. Badawy, E. P. A. M. Bakkers, *et al.*, Probing Majorana localization of a phase-controlled three-site Kitaev chain with an additional quantum dot, Nat Commun **17**, 2313 (2026).

[18] C.-X. Liu, S. Miles, A. Bordin, S. L. D. ten Haaf, G. P. Mazur, A. M. Bozkurt, and M. Wimmer, Scaling up a sign-ordered Kitaev chain without magnetic flux control, Phys. Rev. Res. **7**, L012045 (2025).

[19] J. Alicea, New directions in the pursuit of Majorana fermions in solid state systems, Rep. Prog. Phys. **75**, 076501 (2012).

[20] C.-X. Liu, G. Wang, T. Dvir, and M. Wimmer, Tunable superconducting coupling of quantum dots via Andreev bound states in semiconductor-superconductor nanowires, Phys. Rev. Lett. **129**, 267701 (2022).

[21] A. Bordin, G. Wang, C.-X. Liu, S. L. D. ten Haaf, N. van Loo, G. P. Mazur, D. Xu, D. van Driel, F. Zatelli, S. Gazibegovic, G. Badawy, *et al.*, Tunable crossed Andreev reflection and elastic cotunneling in hybrid nanowires, Phys. Rev. X **13**, 031031 (2023).

[22] See Supplemental Material at http://link.aps.org/supplemental/10.1103/2fyb-mpp9 for additional data and details about experimental and numerical methods.

[23] K. Grove-Rasmussen, G. Steffensen, A. Jellinggaard, M. H. Madsen, R. Žitko, J. Paaske, and J. Nygård, Yu-Shiba-Rusinov screening of spins in double quantum dots, Nat. Commun. **9**, 2376 (2018).

[24] S. Metti, C. Thomas, and M. J. Manfra, Electronic *g* factor and tunable spin-orbit coupling in a gate-defined InSbAs quantum dot, Phys. Rev. B **108**, 235306 (2023).

[25] C. G. Prosko, W. D. Huisman, I. Kulesh, D. Xiao, C. Thomas, M. J. Manfra, and S. Goswami, Flux-tunable Josephson effect in a four-terminal junction, Phys. Rev. B **110**, 064518 (2024).

[26] M. R. Lykkegaard, A. E. Dahl, T. Lindemann, M. J. Manfra, K. Flensberg, and C. M. Marcus, Phase-biased Andreev diffraction grating, Phys. Rev. Lett. **135**, 066301 (2025).

[27] L. Lakic, W. I. L. Lawrie, D. van Driel, L. E. A. Stehouwer, Y. Su, M. Veldhorst, G. Scappucci, F. Kuemmeth, and A. Chatterjee, A quantum dot in germanium proximitized by a superconductor, Nat. Mater. **24**, 552 (2025).

[28] G. Fabris *et al.*, Granular aluminum induced superconductivity in germanium for hole spin-based hybrid devices, arXiv:2602.21364.

[29] M. Coraiola, D. Z. Haxell, D. Sabonis, H. Weisbrich, A. E. Svetogorov, M. Hinderling, S. C. ten Kate, E. Cheah, F. Krizek, R. Schott, *et al.*, Phase-engineering the Andreev band structure of a three-terminal Josephson junction, Nat. Commun. **14**, 6784 (2023).

[30] T. Antonelli, M. Coraiola, D. C. Ohnmacht, A. E. Svetogorov, D. Sabonis, S. C. ten Kate, E. Cheah, F. Krizek, R. Schott, J. C. Cuevas, *et al.*, Exploring the energy spectrum of a four-terminal Josephson junction: Toward topological Andreev band structures, Phys. Rev. X **15**, 031066 (2025).

[31] C. Padurariu and Y. V. Nazarov, Theoretical proposal for superconducting spin qubits, Phys. Rev. B **81**, 144519 (2010).

[32] C. Janvier, L. Tosi, L. Bretheau, Ç. Ö. Girit, M. Stern, P. Bertet, P. Joyez, D. Vion, D. Esteve, M. F. Goffman, *et al.*, Coherent manipulation of Andreev states in superconducting atomic contacts, Science **349**, 1199 (2015).

[33] M. Pita-Vidal, A. Bargerbos, R. Žitko, L. J. Splitthoff, L. Grünhaupt, J. J. Wesdorp, Y. Liu, L. P. Kouwenhoven, R. Aguado, B. van Heck, *et al.*, Direct manipulation of a superconducting spin qubit strongly coupled to a transmon qubit, Nat. Phys. **19**, 1110 (2023).

[34] S. L. D. ten Haaf and W. D. Huisman, Data and code for "Using Andreev bound states and spin to remove domain walls in a Kitaev chain", Zenodo, 2025, doi: 10.5281/zenodo.17857948.